Determining the mechanisms of current flow in structures of two-layer dielectrics

© S.V. Bulyarskiy[1], V.S. Belov[1,2], G.G. Gusarov[1], A.V. Lakalin[1], K.I. Litvinova[1], A.P. Orlov[1]

[1] Institute of Nanotechnology of Microelectronics, Russian Academy of Sciences,
119991 Moscow, Russia
[2] National Research University of Electronic Technology (MIET),
124498 Zelenograd, Russia

E-mail: bulyar2954@mail.ru

Received April 18, 2022
Revised March 10, 2023
Accepted March 10, 2023

Diodes of type Metal-Dielectric 1-Dielectric 2-Metal are promising for use in devices paired with antennas-rectennas. To create diodes with the characteristics required for operation, it is necessary to understand the mechanisms of current transport in both dielectrics and their contacts with metals. To solve this problem, it is necessary to develop an algorithm for dividing the general current-voltage characteristic into characteristics of individual contacts, the analysis of which will also allow us to investigate the problems of the properties of defects in the dielectrics that make up the diode. In this paper, the solution of the above problems is presented on the example of the Al-Al_2O_3-Ta_2O_5-Ni diode. The authors showed how one can divide the current-voltage characteristic into components, calculate potential barriers at the boundaries of metals with contacting dielectrics, and determine the concentration and energy characteristics of structural defects in dielectrics.

Keywords: metal-insulator-metal diodes, current-voltage characteristics, Poole-Frenkel effect, currents of thermionic and thermal field emission, currents limited by space charge.

DOI: 10.21883/SC.2023.02.55958.3545

1. Introduction

In view of the importance of conversion of radiation energy into electrical energy, metal-insulator-metal (MIM) structures, which form a good combination with antennas for reception of electromagnetic radiation, are being studied extensively. A combination of an antenna for reception of radiation energy and a diode, which rectifies alternating current and enables the generation of DC energy, is called a rectenna [1,2]. This may be designed as an energy converter or a detector [3,4]. The low resistance of MIM diodes enables the flow of high-density currents, and their impedance provides a better diode–antenna matching [2,4,5]. Rectennas have certain advantages. For example, they may be integrated directly with MOS structures operating at frequencies up to 95–100 GHz [6] and may operate in the terahertz range [5,7–9]. Since MIM diodes utilize majority carriers and a lack of minority electrons and holes excludes the possibility of recombination, they are well-suited for high-frequency applications and fast switching. These diodes may function in rectennas without an additional power source if metals with different work functions are used for contacts [10–12]. Rectennas with carbon nanotubes are designed to be operated in the optical range of the electromagnetic spectrum [13]. It should be noted that the potential for application of MIM structures at gigahertz and terahertz frequencies is examined mostly theoretically. In real-world contexts, their oxide dielectrics contain a considerable number of defects. These defects produce sticking centers, which are distributed exponentially over the energy, and traps with electron levels that are positioned deep relative to band gaps [14]. Defects induce a significant deviation of the properties of actual diodes from the characteristics of ideal ones. The primary difference consists in an increase in conductivity of the dielectric layer. Therefore, methods for oxide structure diagnostics in finished diodes need to be developed.

The quality of MIM diodes may be improved considerably by introducing a second dielectric. This results in both an improvement of certain characteristics of diodes and an enhancement of asymmetry. The overall thickness of the dielectric layer should remain the same. The asymmetry enhancement is very significant in this design. A diode with two dielectrics allows one to implement resonance tunneling and raise considerably the efficiency of energy conversion [15,16].

At the same time, it was noted in [10] that such MIM diodes have both technological (a thin dielectric layer of a fine quality with a low surface roughness is needed) and design-related drawbacks, which limit the frequency range of their operation. These drawbacks need to be rectified. Therefore, the mechanisms of current flow in these diodes should be studied in order to reveal the causes of the indicated drawbacks (including the high concentration of structural defects, which may contribute to the growth of leakage currents). The electrical characteristics of diodes are an important probe of defect formation processes. The methods for examination of dielectric layers have been characterized well in studies into monolayer homogeneous dielectrics [17,18]. However, certain problems arise in the

case of diodes with two different dielectric layers [19]. One needs to find methods for analyzing the influence of each dielectric layer in such structures on the overall diode parameters. In view of this, the present study is focused on examining the algorithm for determination of the voltage drop across each of the two dielectric layers and analyzing the transport mechanisms in such diodes exemplified by an Al-Al_2O_3-Ta_2O_5-Ni structure.

2. Experimental results

2.1. Fabrication of Al-Al_2O_3-Ta_2O_5-Ni diodes

Al-Al_2O_3-Ta_2O_5-Ni structures were formed on a silicon substrate coated with silicon oxide with a thickness of 600 nm. A 150-nm-thick nickel film (metal 1) was formed on silicon oxide by electron-beam deposition. This film was coated with a 200-nm-thick silicon oxide layer with windows formed in it by photolithography and plasma-chemical etching. A tantalum oxide film was deposited on top of nickel and silicon oxide films by atomic layer deposition. The thickness of deposited tantalum oxide films was measured with an ellipsometer and found to be equal to 3, 5, and 7 nm. An aluminum layer (metal 2) was then formed by electron-beam deposition on top of the tantalum oxide film. The thickness of this layer was 150 nm.

2.2. Auger examination of the stoichiometric composition of Al-Al_2O_3-Ta_2O_5-Ni films

The measured Auger spectra demonstrate that an aluminum oxide layer forms between aluminum and tantalum oxide when aluminum is deposited by an electron beam. Al atoms have a high energy after evaporation and do not only settle down onto the surface of tantalum oxide, but also penetrate deeper into it. Aluminum oxidizes in the process due to the interaction with oxygen of tantalum oxide and facilitates the production of oxygen vacancies in tantalum oxide near the contact. In turn, tantalum oxide becomes depleted in oxygen. Thus, the dielectric layer of a diode after the deposition of aluminum consists of two material layers: aluminum oxide and tantalum oxide.

2.3. High-resolution transmission electron microscopy studies of Al-Al_2O_3-Ta_2O_5-Ni films

Lamellae for high-resolution transmission electron microscopy (TEM) studies were prepared from the fabricated samples. The obtained images reveal several alternating layers: nickel, tantalum oxide, aluminum oxide, and aluminum on top (~ 150 nm). TEM data confirm that the dielectric material is two-layer. An additional aluminum oxide layer with a thickness 2.6 nm formed in samples with tantalum oxide of a varying thickness. Since the same procedure of aluminum deposition was used in the fabrication of samples with different thicknesses of tantalum oxide, the thickness of aluminum oxide remained unchanged and did not depend on the thickness of tantalum oxide. Thus, the dielectric material in the studied structures is two-layer and is composed of tantalum oxide and aluminum oxide with a thickness of 2.6 ± 0.2 nm. Note that the overall thickness of tantalum and aluminum oxide layers exceeds the values determined by ellipsometry. The samples with an ellipsometric thickness of 3 and 7 nm had an overall oxide layer thickness of 4.8 and 8.7 nm, respectively. This is attributable to the expansion of aluminum in the process of oxidation. Since the molar volume of aluminum oxide is 2.5 times higher than the molar volume of aluminum, the film naturally grows thicker as aluminum oxidizes.

2.4. Current–voltage characteristics of Al-Al_2O_3-Ta_2O_5-Ni diodes

The current–voltage characteristics (CVCs) of Al-Al_2O_3-Ta_2O_5-Ni diodes with oxide layers of a varying thickness had the form of CVCs of an asymmetric opposite-barrier structure.

Rectification ratio f_R, which was determined as the ratio of diode current I_{dir} under forward bias to diode current I_{rev} under backward bias at equal voltage magnitudes ($f_R = I_{\text{dir}}/I_{\text{rev}}$), depends on the thickness of tantalum oxide. It reaches its maximum of $\sim 10^3$ in samples with 7 nm of deposited tantalum oxide. As the temperature drops, the rectification ratio decreases and its maximum shifts toward higher voltages.

A high rectification ratio is crucial for diodes used in rectennas. The CVC nonlinearity varies only slightly at voltages greater than 0.2 V. This is also important for diodes used for detection of electromagnetic energy, since nonlinear distortion is suppressed in this case.

3. Algorithm for isolation of current–voltage characteristics of each dielectric

A diode with two dielectric layers has one contact to each of them. A contact to a dielectric always features a potential barrier. Therefore, the differentiation between forward and backward CVCs of such structures is rather arbitrary. The applied external voltage always induces forward and backward bias in the first and the second contacts. This corresponds to a model of two back-to-back diodes [20]. Therefore, it is assumed in the present study that forward CVCs are the ones in which the current varies faster with increasing bias voltage. Two dielectric layers are connected in series for DC current flow. The sum of voltage drops across these dielectrics with their contacts is equal to the voltage applied to the diode.

TEM data demonstrate that the thickness of the aluminum oxide layer remains the same in all samples, while the thickness of tantalum oxide varies. The sum of voltage

drops across these layers is equal to the voltage applied to the diode:

$$U = U_1 + U_2(d), \tag{1}$$

where U_1 is the voltage drop across the aluminum oxide layer, $U_2(d)$ is the voltage drop across the tantalum oxide layer, and d is the thickness of tantalum oxide.

Voltage drop U_1 across aluminum oxide (dielectric 1) depends only on the polarity of the applied voltage and the current magnitude. This voltage is the same for two samples with equal currents flowing through them and different thicknesses of the tantalum oxide (dielectric 2) layer. The voltages at these samples at equal currents are

$$\begin{aligned} U(d_1) &= U_1 + U_2(d_1) \\ &\cdots\cdots\cdots\cdots\cdots \\ U(d_2) &= U_1 + U_2(d_2) \end{aligned}. \tag{2}$$

Let $U(d_2)$ be the voltage drop across the diode with a thicker tantalum oxide layer. Subtracting one expression from the other and taking into account the fact that voltage drop U_1 across aluminum oxide is independent of the thickness of tantalum oxide, we find

$$\Delta U = U(d_2) - U(d_1) = U_2(d_2) - U_2(d_1). \tag{3}$$

One more equation is needed to determine separate voltage drops across tantalum layers of different thicknesses $U_2(d_2)$ and $U_2(d_1)$. The exact form of this equation depends on the mechanism of current flow in tantalum oxide. Until modeling and fitting of the model to experimental data is performed, one can only guess the nature of this mechanism.

Poole–Frenkel effect. It has been noted above that one contact is backward-biased. The current through this contact is then influenced by the effect of potential barrier lowering in an electric field (Poole–Frenkel effect). The essence of the Poole–Frenkel effect is that the electric field of a contact lowers the potential barrier by $\Delta\varphi = \beta_F\sqrt{F}$, where β_F is the Frenkel constant and F is the electric-field intensity. The corresponding expression for current density is written as

$$J_{P-F} = J_S \exp\left(\frac{\beta_F\sqrt{F}}{kT}\right) = J_S \exp\left(\frac{\beta_F}{kT}\sqrt{\frac{U}{d}}\right), \tag{4}$$

where J_S is the current density without the Poole–Frenkel effect, U is the voltage applied to the potential barrier, and d is the barrier thickness, which is equal to the thickness of a dielectric material.

Equating the currents of diodes with different thicknesses of the dielectric material, one finds a simple relation for the voltage drop across layers of different thicknesses:

$$\frac{U_2(d_1)}{d_1} = \frac{U_2(d_2)}{d_2}. \tag{5}$$

Formula (5) also remains valid in the case of other mechanisms of current flow with the bias voltage being in the exponent of a CVC.

Tunnel current. If one assumes that the electric-field intensity is equal to the ratio between the applied voltage and the dielectric layer thickness (U/d), the tunnel current may be written as [17]

$$J = A\frac{U^2}{d^2}\exp\left(-\frac{\gamma d}{U}\varphi_b^{3/2}\right), \tag{6}$$

where A and γ are quantities incorporating universal constants and φ_b is the height of the potential barrier at the metal–dielectric interface. Applying the conditions of equality of currents in samples with different thicknesses and the same potential barrier, we find

$$\frac{d_1}{U_2(d_1)} + \frac{2}{C}\cdot\ln\left[\frac{d_1}{U_2(d_1)}\right] = \frac{d_2}{U_2(d_2)} + \frac{2}{C}\cdot\ln\left[\frac{d_2}{U_2(d_2)}\right]. \tag{7}$$

where $C = \gamma\varphi_b^{3/2}$.

Currents limited by the space charge. The expression for the current density in a dielectric with a monoenergetic trap takes the form

$$J = \frac{9}{8}\varepsilon_S\mu\frac{\Theta}{\Theta+1}\frac{U^2}{d^3}, \tag{8}$$

where $\varepsilon_S = \varepsilon\varepsilon_0$, ε is the relative permittivity, μ is the mobility, and Θ is the ratio of the free carrier density to the net density of (free and trapped) carriers.

The relation between the voltage drops across layers of different thicknesses is written as

$$\frac{U_2(d_1)}{d_1^{3/2}} = \frac{U_2(d_2)}{d_2^{3/2}}. \tag{9}$$

The algorithm is implemented as follows: (1) ΔU is calculated in accordance with (3) based on experimental data; the probable mechanism of current flow is determined. (2) Pairs of formulae corresponding to this mechanism are selected ((3) and (5), (3) and (7), or (3) and (9)), and $U_2(d_1)$, $U_2(d_2)$ are calculated. (3) The obtained result is analyzed.

4. Isolation of current–voltage characteristics of Al-Al_2O_3 and Ta_2O_5-Ni of Al-Al_2O_3-Ta_2O_5-Ni diodes connected in forward bias

4.1. Isolation of current–voltage characteristics of diodes with different thicknesses of tantalum oxide and analysis of the mechanisms shaping these characteristics

An initial assessment of transport mechanisms is made by analyzing the CVCs of a diode plotted in different coordinates.

The CVCs of Al-Al_2O_3-Ta_2O_5-Ni diodes connected in forward bias are presented in Fig. 1.

The CVCs in semi-log scale are nonlinear (Fig. 1, *a*). Therefore, the simple mechanism of thermionic Schottky

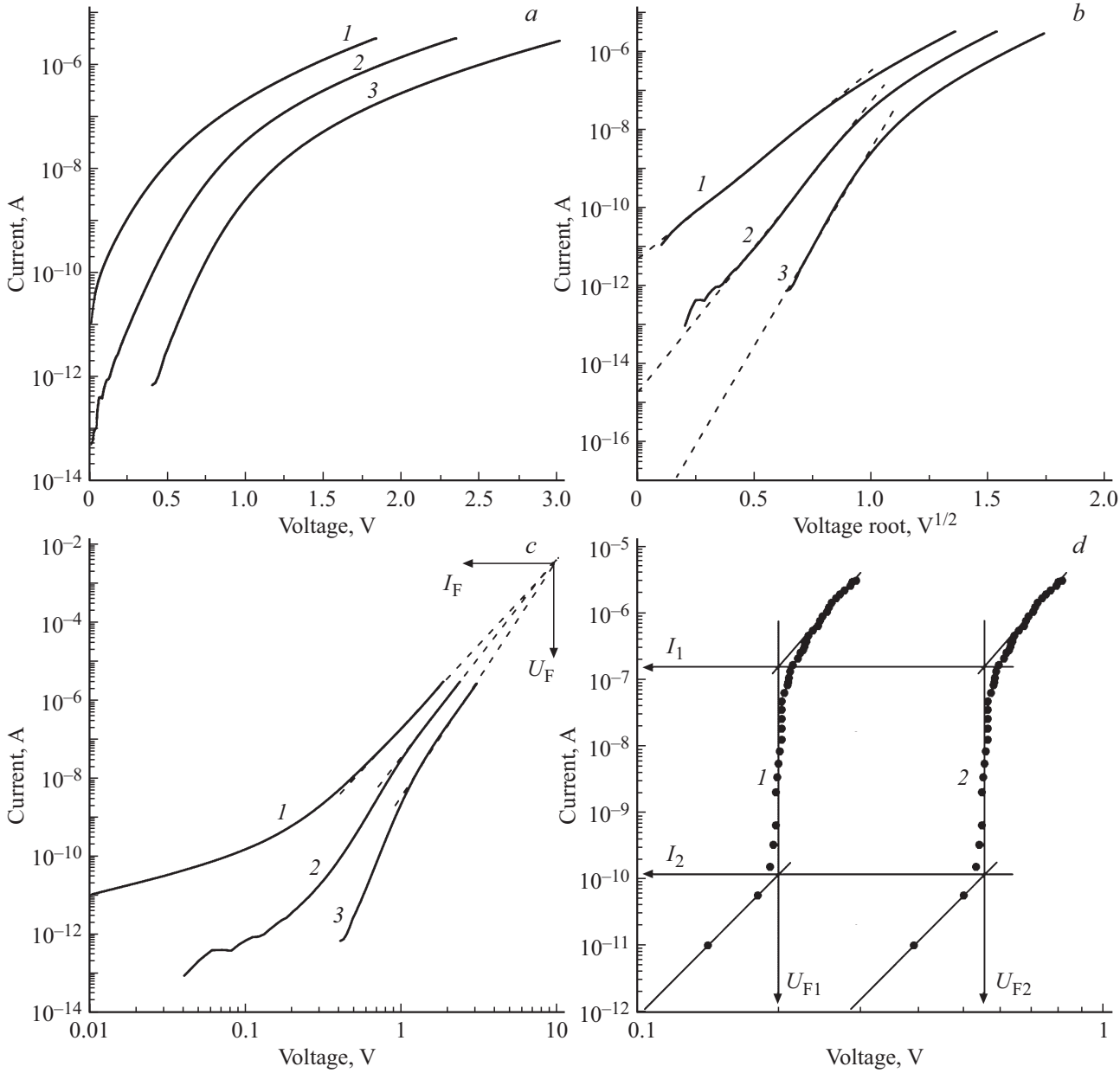

Figure 1. Current–voltage characteristics of Al-Al_2O_3-Ta_2O_5-Ni diodes: *a* — semi-log scale; *b* — semi-log scale, current versus square root of voltage; *c* — log-log scale; *d* — current–voltage characteristic of a Ta_2O_5-Ni contact in log-log scale.

emission is not relevant to the present case. The CVCs in semi-log scale representing the dependence of current on square root of voltage (Fig. 1, *b*) are linear within the initial voltage section. This is typical of the Poole–Frenkel mechanism, which is characterized by formula (4). As the voltage increases further, the characteristics deviate from this dependence. This CVC behavior is indicative of a fairly strong influence of resistance of the bulk of the material. The CVCs in log-log scale are nonlinear within the initial section of bias voltage growth, but then assume a shape typical of currents limited by the space charge with traps distributed in accordance with an exponential law [17]. It follows from preliminary analysis that the Poole–Frenkel transport mechanism shapes the characteristics in the region of high currents. Therefore, Eqs. (3) and (5) are used here to separate the CVCs of an Al-Al_2O_3-Ta_2O_5-Ni diode into Ta_2O_5-Ni and Al-Al_2O_3 components.

The system of Eqs. (3) and (5) was solved for the case when current is governed by overbarrier transport:

$$U_2(d_1) = \Delta U / \left(\frac{d_2}{d_1} - 1\right);$$

$$U_2(d_2) = \Delta U / \left(1 - \frac{d_1}{d_2}\right). \qquad (10)$$

Experimental CVCs under forward bias were replotted using the algorithm detailed in the previous paragraph. The

calculation results for a Ta_2O_5-Ni contact are presented in Fig. 1, *d*.

The data from Fig. 1, *d* indicate that the CVCs of Ta_2O_5-Ni contacts follow the mechanism of currents limited by the space charge. Notably, Ta_2O_5 features two types of energy distribution of traps: a monoenergetic distribution, which shapes the vertical CVC section, and an exponential distribution, which governs the monotonically increasing CVC section [21–23]. The barrier at the nickel–tantalum oxide interface is under forward bias and does not affect the current magnitude. The results reported in [23] were used to calculate the parameters of traps. The voltage of complete filling of traps (U_F) allows one to determine their density [23]:

$$N_t = \frac{\varepsilon_S U_F}{d^2_{Ta_2O_5}}, \qquad (11)$$

where $d_{Ta_2O_5}$ is the thickness of the tantalum oxide layer. The relative permittivity of tantalum oxide is $\varepsilon \approx 26$.

Calculations were performed based on the data from Fig. 1, *d* and the thickness estimate obtained in TEM studies. The results of calculation of N_t are as follows: $1.3 \cdot 10^{20}\,\mathrm{cm}^{-3}$ for a sample with a thickness of 3 nm and $1.2 \cdot 10^{20}\,\mathrm{cm}^{-3}$ for a 5-nm-thick sample. The density of traps distributed over energy is higher and reaches $5 \cdot 10^{20}\,\mathrm{cm}^{-3}$. The activation energy of a monoenergetic trap is written as [23]

$$E_t = kT \ln\left(\frac{N_C I_1}{N_t I_2}\right), \qquad (12)$$

where N_C is the effective density of conduction-band states in tantalum oxide. The values of currents I_1 and I_2 are indicated in Fig. 1, *d*. The result of calculations is $E_t = 0.2\,\mathrm{eV}$. The characteristic energy of the exponential trap distribution may be estimated using the following formula:

$$E_{\exp} = kT_C = k(n-1)T, \qquad (13)$$

where n is the slope of the exponent of the CVC plotted in log-log scale (Fig. 1, *c*). The characteristic energy assumes a value of 0.15 eV.

As was already noted, aluminum oxide forms due to the interaction of aluminum with oxygen taken up from tantalum oxide. It is fair to assume that this induces a high concentration of defects in tantalum oxide in the examined diodes and triggers the emergence of an exponential trap distribution, which is caused by material disordering at a high concentration of defects.

Formula (1) should be used to calculate the CVC of an Al-Al_2O_3 contact. Subtracting the voltage drop at the tantalum oxide–nickel contact from the net voltage drop, one finds the CVC of a contact between aluminum oxide and aluminum, which is presented in Fig. 2.

This CVC is shaped by the Poole–Frenkel mechanism of potential barrier lowering and may be approximated by formula (4) with a Poole–Frenkel constant of $0.0002\,\mathrm{eV} \cdot \mathrm{cm}^{0.5}/\mathrm{V}^{0.5}$, which is close to its theoretical value.

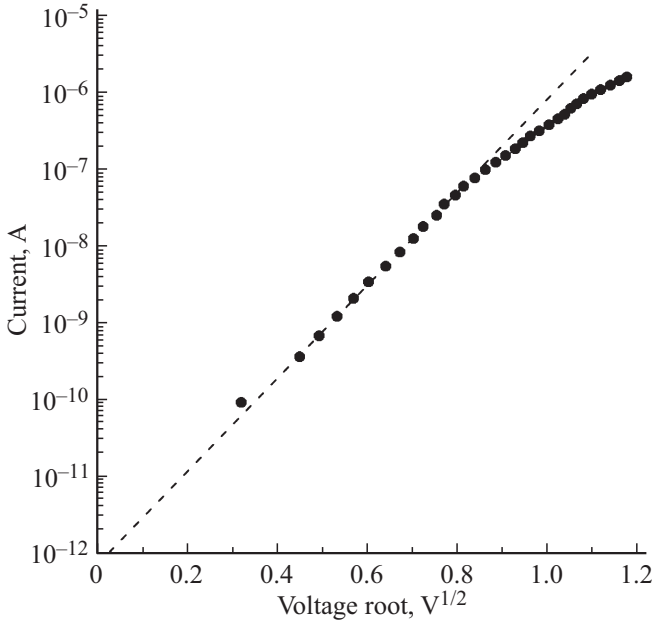

Figure 2. Current–voltage characteristic of an Al-Al_2O_3 contact.

The height of the potential barrier may be estimated by examining the saturation current. The obtained estimate is 0.74 eV. An approximation of this dependence provides an opportunity to separate the CVCs at different temperatures.

4.2. Analysis of the temperature dependences of current–voltage characteristics of Al-Al_2O_3-Ta_2O_5-Ni diodes under forward bias

The temperature dependences of CVCs were studied for diodes with a deposited tantalum oxide layer with an ellipsometric thickness of 7 nm. These samples had the most pronounced asymmetry. Their CVCs are shown in Fig. 3.

The current of Al-Al_2O_3-Ta_2O_5-Ni diodes depends strongly on temperature, and this fact provides evidence of thermionic Schottky emission. The CVC of an Al-Al_2O_3 diode, which is characterized by formula (4), was transformed to isolate the CVC of a Ta_2O_5-Ni diode:

$$I = I_{S1} \exp\left(\frac{\beta_F}{kT}\sqrt{\frac{U_1}{d}}\right) = I_{S1} \exp\left(\frac{\alpha}{T}\sqrt{U_1}\right),$$

$$\alpha = \frac{\beta_F}{k\sqrt{d}}, \quad U_1 = \left[\frac{T}{\alpha}\right]^2 \cdot \left[\ln\left(\frac{I}{I_{S1}}\right)\right]^2, \qquad (14)$$

where U_1 is the voltage drop across an Al-Al_2O_3, I_{S1} is the saturation current of this contact, and T is the measurement temperature.

The voltage drop across an Al-Al_2O_3 contact was calculated in accordance with formula (14) based on the data from Fig. 2. The results of calculations are presented in Fig. 3. This is the CVC of a Ni-Ta_2O_5 contact. It is shaped by the mechanism of currents limited by the space charge

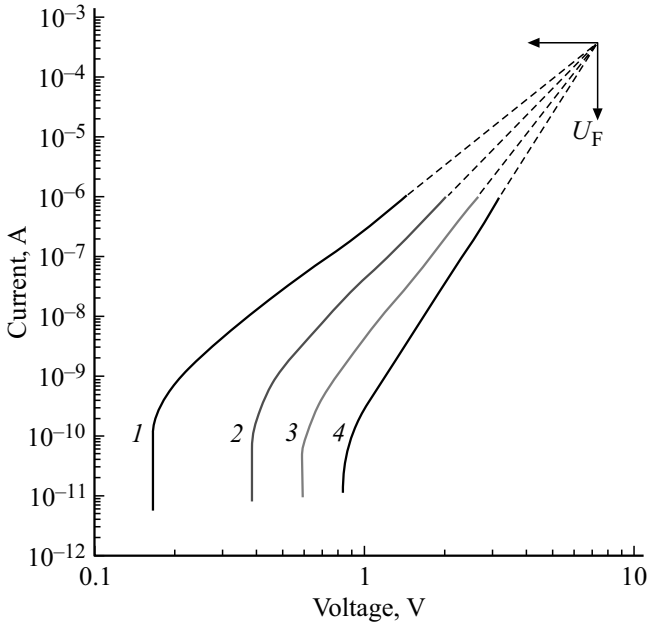

Figure 3. Current–voltage characteristics of a Ta_2O_5-Ni contact after separation with an ellipsometric tantalum oxide thickness of 7 nm. The curves correspond to measurements performed at the following temperatures, K: *1* — 310, *2* — 280, *3* — 250, and *4* — 220.

with a discrete level and a region of levels distributed in accordance with an exponential law (see above).

Thus, the bias voltage polarity inducing a faster current growth with voltage (i.e., the one that was called the forward current) actually sets forward bias of the Ni-Ta_2O_5 contact. The barrier at contact then does not affect the current magnitude, and the current is limited by the space charge in tantalum oxide, which forms the bulk of this contact. The Al-Al_2O_3 contact is backward-biased, and the current through it is governed by the mechanism of potential barrier lowering due to the Poole–Frenkel effect.

5. Current–voltage characteristics of a Ni-Ta_2O_5-Al_2O_3-Al diode under backward bias

The CVCs of Ni-Ta_2O_5-Al_2O_3-Al diodes under backward bias are linear in coordinates $\ln(I) = f(U^{1/2})$. It was hypothesized that these characteristics are shaped by the potential barrier lowering at a backward-biased contact (formula (4)). The values of relative permittivity were calculated for each CVC. They agree well with the relative permittivity calculated using the formula for a plate capacitor and the measured capacitance of Ni-Ta_2O_5-Al_2O_3-Al diodes. At temperatures > 250 K, the permittivity values calculated based on the results of two different experiments match completely. This verifies the applicability of the model of potential barrier lowering to CVCs in the indicated temperature range. The mismatch of data at lower temperatures is indicative of the fact that the mentioned model is inapplicable at these temperatures. The CVCs are parallel at temperatures < 250 K. Both these facts point at a change in the current flow mechanism. Thermionic emission gives way to thermal-field emission, and tunneling processes become more significant.

The permittivity derived from the Poole–Frenkel constant in the region of high temperatures agrees with the value calculated using the formula for a plate capacitor. This permittivity value (26) is the one corresponding to tantalum oxide [24,25]. Therefore, the Ni-Ta_2O_5-Al_2O_3-Al diode current is governed by the Ni-Ta_2O_5 contact current. The height of the potential barrier of this contact may then be calculated based on the saturation current at a temperature of 310 K. The barrier of this contact is 0.87 eV in height.

Thus, the CVCs are shaped exclusively by the potential barrier lowering of the Ni-Ta_2O_5 contact at the examined polarity of the applied voltage in the region of high temperatures. The Al_2O_3-Al contact is forward-biased and does not exert any significant influence on the Ni-Ta_2O_5-Al_2O_3-Al diode current.

6. Conclusion

An algorithm for separation of current–voltage characteristics of diodes with two dielectric layers into individual current–voltage characteristics of contacts M_1-D_1 and M_2-D_2 was developed. It may be applied if the thickness of one dielectric material is constant and the thickness of the other dielectric varies. The application of this algorithm was illustrated using the example of a Ni-Ta_2O_5-Al_2O_3-Al diode. The mechanisms of current flow at different polarities of the applied voltage were also analyzed. With the application of voltage of a certain polarity, the Ni-Ta_2O_5 contact gets forward-biased, while Al_2O_3-Al is backward-biased. The mechanisms of current flow of both contacts were identified in this case. It was demonstrated that the Al_2O_3-Al contact current is controlled by the potential barrier lowering due to the Poole–Frenkel effect, while the Ni-Ta_2O_5 contact current is governed by the mechanism of currents limited by the space charge. This made it possible to determine the energy characteristics and the concentration of defects in tantalum oxide. When direction is reversed, the diode current is specified by the potential barrier lowering of the Ni-Ta_2O_5 contact.

Funding

The study was supported by the Ministry of Science and Higher Education of the Russian Federation, project No. 0004-2022-0004. The investigations were performed in the Institute of Nanotechnology of Microelectronics of the Russian Academy of Sciences (INME RAS) using Large Scale Research Facility Complex for Heterogeneous Integration Technologies and Silicon + Carbon Nanotechnologies.

Conflict of interest

The authors declare that they have no conflict of interest.

References

[1] S. Shriwastava, C.C. Tripathi. J. Electron. Mater., **48** (5), 2635 (2019). https://doi.org/10.1007/s11664-018-06887-9

[2] S. Grover, G. Moddel. IEEE J. Photovoltaics, **1** (1), 78 (2011). https://doi.org/10.1109/JPHOTOV.2011.2160489

[3] M. Heiblum. Solid State Electron., **24**, 4 (1981). https://doi.org/10.1016/0038-1101(81)90029-0

[4] G. Moddel, S. Grover. *Rectenna Solar Cells* (Springer, 2013). https://doi.org/10.1007/978-1-4614-3716-1

[5] E. Donchev, J.S. Pang, P.M. Gammon, A. Centeno. MRS Energy Sustainab., **1** (1), 1 (2014). https://doi.org/10.1557/mre.2014.6

[6] E. Shaulov, S. Jameson, E. Socher. *2017 IEEE MTT-S Int. Microw. Symp.*, 307 (2017). https://doi.org/10.1109/MWSYM.2017.8059105

[7] M. Dragoman, M. Aldrigo. Appl. Phys. Lett., **109** (11), 113105 (2016). https://doi.org/10.1063/1.4962642

[8] A. Costanzo, M. Dionigi, D. Masotti, M. Mongiardo, G. Monti, L. Tarricone, R. Sorrentino. Proc. IEEE, **102** (11), 1692 (2014). https://doi.org/ 10.1109/JPROC.2014.2355261

[9] I. Wilke, Y. Oppliger, W. Herrmann, F. Kneubühl. Appl. Phys. A: Mater. Sci. Process., **58**, 329 (1994). https://doi.org/10.1007/BF00323606

[10] A.A. Khan, G. Jayaswal, F.A. Gahaffar, A. Shamim. Microelectron. Eng., **181**, 34 (2017). https://doi.org/10.1016/j.mee.2017.07.003

[11] S. Joshi, G. Moddel. IEEE J. Photovoltaics, **6** (3), 668 (2016). https://doi.org/10.1109/JPHOTOV.2016.2541460

[12] M.N. Gadalla, M. Abdel-Rahman, A. Shamim. Sci. Rep., **4**, 4270 (2014). https://doi.org/10.1038/srep04270

[13] E.H. Shah, B. Brown, B.A. Cola. IEEE Trans. Nanotechnology, **16** (2), 230 (2017). https://doi.org/10.1109/TNANO.2017.2656066

[14] G. Pacchioni, S. Valeri. *Oxide Ultrathin Films* (Wiley-VCH Verlag GmbH & Co., 2012).

[15] F. Aydinoglu, M. Alhazmi, B. Cui, O.M. Ramahi, M. Irannejad, A. Brzezinski, M. Yavuz. Austin J. Nanomed. Nanotechnol., **1** (1), 3 (2014). https://ece.uwaterloo.ca/ bcui/ Publication/2014%20MIM%20diode%20Ferhat%20AJNN.pdf

[16] A. Belkadi, A. Weerakkody, G. Moddel. Nature Commun., **12**, 2925 (2021). https://doi.org/10.1038/s41467-021-23182-0

[17] Fu-Chien Chiu. Adv. Mater. Sci. Eng., Article ID 578168 (2014). http://doi.org/10.1155/2014/578168

[18] T.-H. Chiang, J.F. Wager. IEEE Trans. Electron. Dev., **65** (1), 223 (2018). http://doi.org/10.1109/TED.2017.2776612

[19] S. Grover, G. Moddel. Solid State Electron., **67**, 94 (2012). https://doi.org/10.1016/j.sse.2011.09.004

[20] S.V. Bulyarskii, O.A. Nevskii, G.E. Zhelyapov. FTP, **15** (7), 1660 (1981) (in Russian).

[21] A. Rose. Phys. Rev., **97**, 1538 (1955). https://doi.org/10.1103/PhysRev.97.1538

[22] M.A. Lampert. Phys. Rev., **103**, 1648 (1956). https://doi.org/10.1103/PhysRev.103.1648

[23] M.A. Lampert, P. Mark. *Current Injection in Solids* (N.Y.-London, Academic Press, 1970).

[24] S. Ezhilvalavan, T.Y. Tseng. J. Mater. Sci.: Mater. Electron., **10**, 9 (1999). https://doi.org/10.1023/A:1008970922635

[25] G. Aygun, R. Turan. Thin Sol. Films, **517** (2), 994 (2008). https://doi.org/10.1016/j.tsf.2008.07.039

Translated by D.Safin